Main manuscript for

Xenosiderophore transporter gene expression and clade-specific filamentation in *Candida auris* killifish infection

Hugh Gifford[a], Tina Bedekovic[a], Nicolas Helmstetter[a], Jack Gregory[a], Qinxi Ma[a], Alexandra C. Brand[a], Duncan Wilson[a], Johanna Rhodes[b,c], Mark Ramsdale[a], Tetsuhiro Kudoh[d,1], Rhys A. Farrer*[a,1]

[a]MRC Center for Medical Mycology, University of Exeter, Geoffrey Pope Building, Stocker Road, Exeter, United Kingdom, EX4 4QD

[b]Department of Medical Microbiology, Radboudumc, Geert Grooteplein Zuid 10, Nijmegen, Netherlands, 6525 GA

[c]MRC Centre for Global Infectious Disease Analysis, Imperial College London South Kensington Campus, London, United Kingdom, SW7 2AZ

[d]Biosciences, University of Exeter, Geoffrey Pope Building, Stocker Road, Exeter, United Kingdom, EX4 4QD

[1]Co-Senior Author

Corresponding Author: Rhys Farrer

Email: R.Farrer@exeter.ac.uk

Author contributions: Designed research: All authors. Performed research: HG, TB, NH, JG, QM. Analysed data: HG. Wrote the paper: All authors.

Competing interest statement: No competing interests.

Classification: Biological sciences, Microbiology.

Pre-print: This article has been previously made available as a pre-print *via* the bioRxiv server.

Keywords: *Candida auris*, *Aphanius dispar*, dual host-pathogen RNA-seq, siderophore transport, filamentation

This PDF file includes:

Main text

Figures 1-4

Abstract

Candida auris is a World Health Organization (WHO) critical priority fungal pathogen. An associated mortality of ~45%, rising drug resistance and massive nosocomial outbreaks complicate clinical treatment. A critical bottleneck in understanding virulence is the lack of gene expression profiling models during *in vivo* host tissue infection. We developed a thermo-relevant fish embryo yolk-sac (*Aphanius dispar*; Arabian killifish; AK) microinjection model at human body temperature featuring clinically relevant features of host immunity. This allowed us to interrogate infection dynamics through dual host-pathogen RNA-seq at 24 and 48 h post injection (HPI) at 37 °C across five major clades (I-V) of *C. auris*. Host responses to infection featured heat shock, complement activation, and nutritional immunity, including haem oxygenase (*HMOX*) expression in response to clade IV infection. We identified an *in vivo* transcriptional signature across five clades of *C. auris* that was highly enriched for putative xenosiderophore transmembrane transporters. We describe this newly-discovered seventeen-member xenosiderophore transporter candidate (*XTC*) family in terms of individual gene expression patterns, and a sub-clade of five putative haem transport-related (*HTR*) genes. Only the basal clade V isolate formed filaments during infection, coinciding with typical and atypical regulators of morphogenesis, including *UME6*, *HGC1*, and the novel adhesin *SCF1*. Clades I and IV demonstrated increased virulence, coinciding with up-regulation of three *HTR* genes in clade IV, and the mating-type locus (*MTL*) non-mating gene *PIKA* in both. Our study provides critical insights into the pathogenesis of C. auris, including species-wide up-regulation of *XTC* and *HTR* genes during clinically relevant *in vivo* host tissue infection.

Significance statement

Candida auris is an emerging human fungal pathogen and global public health threat, but *in vivo* tissue infection transcriptome analysis has not been achieved with available models. We infected Arabian killifish yolk-sacs to study gene expression programmes by five clades of *C. auris*. We discovered that the basal clade V uniquely filamented during infection. Additionally, all clades encode a large expanded family of xenosiderophore transporters that are upregulated during infection. These results highlight the important roles for morphology switching and iron acquisition during infection, both of which shed light on its mechanisms of infection and could make novel drug targets.

Main text

Introduction

C. auris is an ascomycetous yeast that has rapidly transitioned from recent emergence to global public health threat (1) and World Health Organization (WHO) critical priority human fungal pathogen (2). The oldest known historical isolate is from 1996 (3) and it was first recognised as a species in 2008 (4).

Over the last decade, *C. auris* had caused nosocomial outbreaks globally resulting in intensive care unit (ICU) shutdowns and massive infection control costs (5–7). Worryingly, *C. auris* is now a leading cause of invasive candidiasis in several hospital settings globally (8, 9). Distinct clades of *C. auris*, including a recent sixth clade (10, 11), suggest that multiple populations of *C. auris* have simultaneously emerged from an unknown niche, all of which are highly adapted for human infection (12, 13). Clade-specific differences have been noted, including clades I, III, and IV more commonly associated with invasive disease and nosocomial outbreaks, while clades II and V have been primarily reported in cases of otomycosis and rarely in bloodstream infection (14). Human mortality associated with *C. auris* candidaemia is potentially higher with clades I and IV than clade III, but this difference has not been shown to be statistically significant (15). Clade and strain-specific genotypic and phenotypic variation may underlie differences in clinical presentation and pathogenesis.

C. auris bloodstream infection is associated with a human mortality of ~45% (16). Owing to the recency of its emergence, the factors governing in-host fitness and virulence during infection are poorly understood. *C. auris* has been shown to reproduce as budding yeasts in mammalian tissues (17, 18) and possess multiple adhesins associated with an aggregation phenotype (19, 20). There has been no evidence of toxin synthesis unlike distantly related *C. albicans* (21, 22). *C. auris* digests of host tissue through secreted aspartyl proteases (23) and evades host immune responses through cell surface masking (24) and intra-phagocytic survival with cell lysis (25). *C. auris* also demonstrates high rates of azole antifungal drug resistance and a rising incidence of pan-drug resistance (26).

Gene expression profiling has become a standard approach for assessing host and pathogen responses to infection. However, no experiment has described the gene expression of *C. auris* during *in vivo* infection of living tissue to date. Studies assessing the transcriptome in an *in vivo* murine catheter model (27), human whole blood *ex vivo* (28), co-incubation with human dermal fibroblasts (29) or murine cell line-derived macrophages (30) have been informative. Additionally, host responses have been assessed in murine peripheral skin (31), human peripheral blood-derived monocytes (32), and murine bone marrow-derived macrophages (33). However, these studies have not reported adequate pathogen RNA recovery to interrogate in-host pathogen expression, except for the dual RNA-seq study using the *ex vivo* whole blood model, for which it was possible to compare gene expression profiles between *C. auris* and other *Candida* species (28).

The dearth of studies profiling host-pathogen gene expression *in vivo* for *C. auris* infection may relate to the lack of a model which allows adequate RNA recovery, balanced with a reasonable degree of clinical relevance. Most murine models, such as BALB/c (17, 34–36) and C57BL/6 mice (33), have only very rarely demonstrated lethality through *C. auris* infection (32, 37, 38) without major

immunosuppression with cyclophosphamide/cortisone (39–50), monoclonal antibody neutrophil depletion (18, 51), or other immunodeficiency (19, 52, 53). Additionally, mouse models are also expensive and associated with concerns over environmental pathogen shedding (54). Alternative host models such as *Galleria mellonella* (34, 44, 55–61), *Drosophila melanogaster* (62) and *Caenorhabditis elegans* (60) have been employed, but these may lack key elements of mammalian-relevant immune systems, thus limiting their scope of application. In patients, immune control of *C. auris* is thought to depend on myeloid cell activity *via* C-type lectin receptors such as complement receptor 3 and mannose receptor MMR, followed by interleukin (IL)-17 pathway activation (63, 64). Therefore, an animal model that aligns with these mechanisms will assist human-relevant profiling of host-pathogen interactions.

Fish larvae must survive hostile and varied ocean environments, demonstrating very early innate immune responses such as antimicrobial peptide production and the complement cascade (65, 66). Only in adulthood are teleost fish expected to possess functional IL-17 subtypes (A and F) that lead to T-helper-17 subset differentiation and adaptive immunity in response to fungal infection (67). The zebrafish (*Danio rerio*) model has allowed hindbrain (24, 68) and swim bladder (69) microinjection modelling of *C. auris* infection, but rarely at temperatures above 30 °C, which zebrafish are broadly intolerant of. There have been no in-host transcription studies using the zebrafish model. Fungal transcriptional programmes can vary greatly across temperatures and are critical for mammalian pathogenesis (70–72). A thermotolerant teleost fish embryo model such as the *Aphanius dispar*, also known as the Arabian killifish (AK), which can acclimatise to temperatures up to and including 40 °C (73–76), offers a balance between considerations of suitability for experimental manipulation and applicability to human fungal infection at mammalian temperatures.

The environmental origins of *C. auris* have not been conclusively demonstrated. However, a marine origin has been hypothesised and supported by successful isolation of *C. auris* in coastal waters of both Indian and Pacific oceans (77, 78). Notably, a close relative of *C. auris* in the *Metschnikowiaceae* clade, *C. haemulonii*, was first isolated in 1961 from the gut of blue-striped grunt (genera name "*Haemulon*" for their blood-red mouth interior) (79). Therefore, a marine model could shed light on a possible evolutionarily adaptive niche relevant not only to human infection but also to hypothetical origins in an emerging pathogen. Additionally, fish embryo models align with the principles of replacement, refinement and reduction of animals in laboratory research and offer a opportunity to develop novel clinically relevant models with ethical benefits over models such as adult mice (80).

In this paper, we present the first study exploring in-host virulence of *C. auris* clades I-V in the AK yolk-sac microinjection model at 37 °C. We supplemented our validation of the model with histology, fungal burden recovery, and dual host-pathogen RNA-seq. By comparing *in vivo* and *in vitro* expression

profiles of *C. auris*, we detected a cross-clade expression signature that was significantly enriched for siderophore transporter *SIT1* paralogues, which mediate uptake of siderophores produced by other microbes (xenosiderophores). We designated this expanded gene family as xenosiderophore transporter candidates (*XTC*), which included a haem transport-related (*HTR*) sub-clade. We also identified *in vivo* filamentation by clade V during infection, which was associated with orthologues of key hypha-associated genes from *C. albicans*. Together, these findings substantially enhance our knowledge of the processes employed by *C. auris* during infection.

Results

Our AK yolk-sac microinjections with each of the five *C. auris* clades demonstrated lethality (defined by cessation of heartbeat, **Figure 1A**) at 37 °C (92-100% *vs* 6% for sham injections). *C. auris* was significantly more lethal at earlier timepoints for clade I (*vs* II, III or V) and clade IV (*vs* II or III), with $p < 0.001$ and $p < 0.04$ respectively (**Figure 1B**, **Table S1**). We compared histological sectioning of *C. auris* in the AK yolk-sac at 48 HPI to understand morphological consequences of *C. auris* infection. All clades of *C. auris* grown *in vitro* and *in vivo* exhibited budding yeast morphologies, except for the clade V strain, which demonstrated predominantly filamentous forms grown *in vivo* (**Figure 1C**). Only minor inter-clade differences were recorded for growth rate and counts of colony-forming units (CFU). Specifically, clade II was slower growing in YPD-broth at 37 °C (**Figure S1A**), a difference that was not later identified in CFUs recovered from infected AK embryos (**Figure 1D**). A mean average (x) of 673 CFUs were recovered per infected embryo, which increased 166x 24 h post injection (HPI, $x = 1.12 \times 10^5$) and a further ~60% after 48 HPI ($x = 1.78 \times 10^5$). Filamentous clade V colonies were then grown on YPD-agar, demonstrating rough (as opposed to smooth) colonies in approximately 1-2% of plated colonies (**Figure S1B**), which consisted of elongated yeast cells and filamentous structures (>10-50 µm) consistent with pseudohyphae (**Figure S1C**). These results indicate that AK embryo yolk-sac microinjection is resulting in an active *C. auris* infection, which is associated with death after 7 d, and therefore is an informative model for the study of human fungal pathogens such as *C. auris*.

To characterize host responses to *C. auris* during infection, we identified host differentially expressed genes (DEGs) between infection by each clade and sham injections. We identified 685 DEGs during infection with any clade (2.49% potential genes), of which 183 were up-regulated and 508 were down-regulated in response to at least one clade. There were no host DEGs common to infection by all five clades. Only four up-regulated genes and one down-regulated gene was shared across host responses to four clades of infection (**Table S2**). Up-regulated genes in 4/5 clades included Laminin subunit alpha-1 (*LAMA1*), Glucose-6-phosphatase (*G6PC*), DN117939 (hypothetical protein) and Tryptophan aminotransferase protein 1 (*TAR1*). The immunoglobulin-like fibronectin type III domain-

containing protein 1 (*IGFN1*) was down-regulated in 4/5 clades. These results suggest AK larvae have only a subtle non-uniform response to each clade of *C. auris* microinjection at these time-points, also potentially reflecting differences in virulence between strains and stages of infection.

While a common host response to all clades of *C. auris* was not identified, we did identify clade-specific host responses to infection. At 24 HPI, clade II elicited the greatest host response, with 41 up-regulated genes and 210 down-regulated genes (**Figure 2A**). Reassuringly, we detected very few differences between sham injection and no injection (**Figure 2B**, SI Appendix). At 48 HPI, clade IV elicited the greatest host response, with 49 up-regulated genes and 104 down-regulated genes). Importantly, we found differential expression of heat shock proteins (*HSP30* and *HSP70*), complement cascade elements, pattern recognition receptors (PRRs), inflammatory transcription regulators, and modulators of nutritional immunity with higher log-fold changes in clades I and IV, especially at 48 HPI (**Figure 2C**). The most prominent gene relevant to pathogen recognition was *CARD14* in clade I and IV infection at 48 HPI (**Figure 2D-E**). We found *NLRP3* (inflammasome) expression during clade III infection at 24 HPI. Several significantly enriched functional terms were identified from our DEGs, especially among the more virulent clades I and IV at 48 HPI. Host transcriptional response to clade I infection included 15 enriched GO terms, driven by up-regulation of two orthologues of *LAMA1* and *LAMA2* (**Figure 2D**). Clade IV had significant changes in functional annotation related to haem catabolism, haem binding, and haem oxygenase (*HMOX*). Two orthologues of *HMOX* drove most of these enrichments, such as haem oxidation (log-fold change x = 3.96, FDR < 0.0003, **Figure 2E**, **Figure S2**). Another host up-regulated gene from infection by clade IV was ferroxidase hephaestin (*HPHL1*), which is also involved in iron nutritional immunity. Together, these findings suggest that heat shock proteins, nutritional immunity (particularly iron acquisition), and the complement effect system are important elements of the AK larval response to *C. auris*.

We compared the in-host transcriptome to expression induced by growth in a standard rich laboratory media (YPD). Principle components and sample correlation clustering from gene expression data indicated a predominant separate clustering of *in vivo vs in vitro* conditions, indicating that the gene expression profile of *C. auris* during infection is substantially different to that when it is grown in nutrient-rich laboratory media (**Figure S1G and S1H**). We identified 960 DEGs between *in vivo* AK infection at 24 HPI or 48 HPI *vs in vitro* culture in YPD over 24 h (499 up-regulated, 523 down-regulated, 17.7% of potential genes, **Figure 3A**). We identified few DEGs between the two time-points 24 HPI to 48 HPI, with zero DEGs for clade IV and V between those time points (**Figure S3A**). The highest numbers of up-regulated DEGs were identified in the filamentous clade V at 24 HPI and in the more virulent clades I and IV at 48 HPI (**Figure S3B-C**). Six functional annotation terms were enriched across all in-host infections at 48 HPI, related to major superfacilitator family carbohydrate and siderophore-iron transmembrane

transport (**Figure S4**). Together, this analysis reveals that during infection, which is a nutrient-limited environment, *C. auris* is responding by significantly increasing expression of genes involved in sugar uptake, as well as members of the *C. auris* expanded gene family of siderophore transporters.

Thirteen DEGs common to all clades of in-host transcription were transmembrane transporters, including up-regulation of transporters for xenosiderophores (*SIT1* genes 3921 and 1487), sugar transporters (*HGT2*, *HGT12*), an ammonia transporter (*ATO2*), and a nicotinic acid transporter (*TNA1*). We also found down-regulation of several drug-resistance-related efflux pumps (*MDR2* and *DTR1*) and peptide transporters (*TPO3*, *PTR22*, **Figure 3B**, **Table S3**). Surprisingly, several putative virulence factors such as lipase *LIP1* and cell wall-related *KRE6* and *SOD6* were also down-regulated across all five clades, as were *ALS4* and *MDR1* in at least one clade (**Figure 3C**). Several members of the *SIT1* family were differentially expressed by <5 of the clades including 0002, 1457, 1458, 1542,2110, 2241, 2465, 3908 and 4097. Meanwhile, two *SIT1* genes were down-regulated across 3 of the clades (1519 and 1499). Several *SIT1* genes were upregulated in ≥1 clade and down-regulated in ≥1 clade (3908 and 2465). The strong signal of differential expression in the *SIT1* expanded gene family highlights the potential importance during in-host survival.

The more virulent clades (I and IV) are **a**-type mating type locus (*MTL*), while the less virulent clades (II, III and V) contain the **α**-type *MTL*. Surprisingly, we found differential expression in several non-mating genes between more virulent and less virulent clades, including poly-A polymerase (*PAP1*), oxysterol binding protein (*OBPA*) and phosphatidylinositol 4-kinase (*PIKA*, **Figure S5B**). Within the set of 10 DEGs shared across all comparisons, several genes outside the *MTL* were up-regulated, including vacuolar protein sorting gene, *VPS70*, and filamentous growth regulator, *FGR14*. Additionally, the drug efflux pump, *MDR1*, was down-regulated across all comparisons, supporting the idea of a fitness trade-off between resistance and virulence.

To explore drivers of filamentation by the clade V strain, we identified 1,046 DEGs between clade V and each of the other clades (I-IV), comprising 601 up-regulated and 526 down-regulated genes across all comparisons. We identified a set of 57 genes shared across all comparisons for *in vivo* conditions only, since we did not observe filamentation in nutrient-rich YPD. Twenty-two genes were up-regulated at 24 HPI, seven at 48 HPI, and 18 at both time-points (**Figure S5C**). Most of the up-regulated genes were metabolic (n = 13), including two cytochrome P450 *ERG5* orthologues, though *ERG11* was down-regulated. Transmembrane transporters for sugar (including two *HGT13* orthologues), amino acids and siderophores (*SIT1* 1487) were also up-regulated (n = 10). Cell wall genes up-regulated in filamentous clade V (n = 8) included the novel adhesin *SCF1*, GPI-anchored genes *PGA31* and *IFF4*, and orthologues of classical *C. albicans* hyphal adhesins *ALS3* and *RBR3*. We identified differentially expressed

transcription factors and related regulators, such as *HAP41* and the pheromone receptor *STE2*, which could play a governing role on these responses.

We examined significant DEGs between clade V and at least one other clade using mean-log fold change (**Figure S5D**). Several genes that play critical roles in *C. albicans* hypha formation were highly up-regulated, such as transcription factor *UME6* and hypha-specific G1 cyclin-dependent protein serine/threonine kinase *HGC1*. Enrichment analysis indicated up-regulated gene sets involving CFEM domain, cytochrome P450/oxidoreductase activity, hypha-regulated cell wall GPI-anchored proteins and siderophore transport, particularly at 24 HPI and comparing clade V to clade II (**Figure S5D**). Significantly up-regulated iron-related transport genes in clade V included *FRE3*, *CFL4*, *FRP1*, and *SIT1* genes 1487, 1499, 1519, 1542, and 4097. This is consistent with the preservation of a major filamentation programme in *C. auris*, demonstrated in the basal clade V.

Given the prominence of *SIT1* orthologues across the transcriptomic analyses of *C. auris* during *in vivo* gene expression, we set out to characterise the structural and evolutionary conservation of the expanded gene family across orthogroups, including outgroup species *C. haemulonii* and *C. albicans*. We performed phylogenetic analysis on proteins with sequence similarity across seven orthologue clusters, of which two main groupings of transporters with 14 transmembrane domains (TMRs) emerged (**Figure S6**). The first group included genes with functional annotation relating to siderophore import (including 12 genes in clade I). The second group included haem transmembrane import genes (including 5 genes in clade I). Most of the orthologues retained 14 TMRs, and few had evidence of additional annotations except for the trichothecene mycotoxin efflux pump PFAM domain across multiple groupings. The orthologue *SIT1* 1547 contained 12 TMRs and was up-regulated with *SIT1* 1548 containing 2 TMRs, which was not identified as a *SIT1* orthologue in our pipeline but has previously been described as such (28, 81).

To explore the evolutionary history of *SIT1*-related genes in fungi, we identified 1,689 homologs of *C. albicans SIT1* across 304 reference genomes from 226 fungal species, which clustered into two branches: a smaller branch annotated for siderophore transport including the 12 *C. auris* groupings which we have designated “xenosiderophore transporter candidates” (*XTC*), and a larger branch featuring genes predicted (by GO term) to encode haem transporters, including the 5 *C. auris* groupings, which we have additionally designated “haem transport-related” (*HTR*, **Figure 4A**). There were no putative haem transporters or members of the larger branch for *C. albicans*, which only contained the single *SIT1* gene. The most prominent expansion of the *XTC* branch in the *Metschnikowiaceae* clade was in *C. haemulonii* (n = 15), followed by *C. auris* (n = 12). *XTC* orthologues were not present in any members of the basal *Blasocladiomycota*, *Chytridiomycota* and *Mucoromycota*, or in several *Ascomycota* (e.g. *Pichia*

kudriavzevii, *Schizosaccharomyces pombe* and *Pyricularia oryzae*) and Basidiomycota (e.g. *Ustilago maydis*). Common human fungal pathogens such as *Aspergillus fumigatus*, *C. albicans* and *Nakaseomyces glabratus* contained only one *XTC* orthologue (**Figure 4B**). The *HTR* clade, by contrast, was more prominent across fungal phyla, with as many as nine in *Mucor* species, 16 in *A. flavus* and 22 in *F. solani*. We therefore propose a naming of these two expanded gene families as *XTC1-12* and *HTR1-5* in *C. auris*.

C. auris demonstrates clade-specific *XTC* presence-absence polymorphisms including the absence of *XTC5* in clade V, *XTC10* in clade IV, and *XTC4*, *XTC9* and *XTC11* in clade II (**Figure 4C**). Clade II exhibited the greatest degree of *XTC* gene loss. Additionally, the AK embryo expressed *HMOX* genes during clade IV infection, while clade IV up-regulated *HTR1*, *HTR2* and *HTR5*. This suggests a specific host-pathogen interaction axis in nutritional immunity related to haem scavenging. No other clades of infection were associated with such iron-related functional enrichment in the host, and no other clades expressed more than one *HTR* gene. Overall, eleven *XTC* genes were differentially expressed in-host compared to *in vitro* growth, including up-regulation of *XTC1*, *XTC2*, *XTC3*, *XTC4*, *XTC6*, *XTC7*, *XTC11* and *XTC12*, and down-regulation of *XTC8*, *XTC9* and *XTC12* in at least one clade. In-host up-regulation of *XTC3* and *XTC7* was significant across all clades. Additionally, the more virulent clades were associated with up-regulation of *XTC4*, *XTC5*, and *XTC8*. The filamentous clade V up-regulated *XTC7* across comparisons with all other clades, and up-regulated *XTC1*, *XTC4*, *XTC8* and *XTC9* compared to at least one other clade.

Discussion

We have described a model for comparative functional genomics of *C. auris* in-host survival using AK yolk-sac microinjections at a clinically relevant temperature in living tissue of a host featuring mammalian-relevant innate immunity. All five clades demonstrated lethality, with a increase in virulence during clades I and IV infections, consistent with clinical and laboratory findings (15). In-host growth was similar across all clades and high enough to indicate a large enough *in vivo* fungal burden for robust bulk transcriptome interrogation across the species. The contained nature of the yolk-sac provides a host tissue growth medium that enables the assessment of pathogen survival and virulence strategies *in vivo* and a straightforward experimental unit of host tissue without the challenges of pathogen RNA isolation such as locating foci of infection in larger animals. Additional time-points could be an informative future area of study to develop fine-resolution strain-specific transcription networks. Furthermore, the potential of a translucent and genetically tractable fish embryo model could enable future visualisation of cellular dynamics and genetic pathway manipulation (74). Thus, an AK yolk-sac microinjection model has the

potential to fill a substantial need for *in vivo* gene expression studies in general.

We investigated the host transcriptional response to *C. auris* infection, which featured an innate immune response, as expected. The most highly up-regulated gene family included two haem oxygenase (*HMOX*) genes. *HMOX* genes have been shown to mask iron from invading pathogens as a feature of anti-*Candida* nutritional immunity (82), so presumably have a similar function against *C. auris*. This was particularly notable given *HMOX* genes were up-regulated in response to clade IV infection, and the clade IV isolate had a corresponding significant up-regulation of 3 haem transport-related *HTR* genes. In addition to nutritional immunity genes, we found up-regulated heat shock and complement cascade genes during infection, confirming the expected immune response to fungal infection (63, 64). Genes with complex roles in immunity were up-regulated, such as *NLRP3*, for which *C. auris* may be less activating than e.g. *C. albicans* (25, 83). It is notable that the yolk-sac model was not associated with histological or transcriptional evidence of host neutrophil recruitment and activation, which may relate to the hypothesis that *C. auris* is immunoevasive (31). Reference genome bias resulting from the available adult gill transcriptome assembly (84) may limit detection of host gene expression features, so future long and short read assembly from gene expression data across a range of larval stages could further understanding of AK immunity.

We provided a thorough investigation of differential expression by *C. auris* during infection of host tissue compared with *in vitro* conditions for the first time. The lack of a major distinction across time-points (24 *vs* 48 HPI) indicates that the transcriptional activity of *C. auris* in-host was highly similar at these stages. Six functional annotation terms (GO, KEGG pathway and PFAM domain) were significantly enriched among genes that were up-regulated across all five clades, including sugar and siderophore transporters. The enrichment of sugar transporters outside of nutrient-rich YPD-broth is unsurprising, such as high-affinity glucose transporter *HGT12*, with evidence of redundancy in *C. albicans* (85–88), and *HGT2*, part of an eight-gene “core filamentation response network” in *C. albicans* (89). More surprising was the down-regulation of putative virulence factors such as Secreted Aspartyl Protease 3 (*SAP3*), thought to be the most important SAP in *C. auris*, and required for virulence in a mouse model (23), and Copper Superoxide Dismutase *SOD6*, which has been shown to be down-regulated in iron starvation (90). Multi-drug efflux pumps such as *MDR2* (down-regulated *in vivo*) and *MDR1* (down-regulated *in vivo* and in clades I and IV *vs* clades II and III) are understood to drive drug resistance through multiple but unclear mechanisms in *C. auris* (91, 92); in-host down-regulation may indicate a fitness trade-off for virulence *vs* drug resistance.

Mating type locus (*MTL*) genes have been hypothesised to contribute to virulence in fungal species including *Cryptococcus neoformans* (93). Given that *C. auris* is assumed not to undergo meiotic

recombination (94), there is a question of what role *MTL*-associated genes play in pathogenesis and morphology. Two of the three non-mating genes (*PAP1* and *PIKA*) in the *MTL* were up-regulated by more virulent strains (I and IV) compared to the less virulent strains (II and III). Importantly, the two more virulent clades (I and IV) contain *MTL**a*** rather than *MTL**α*** (clades II & III) (21), and clades V and VI contain *MTL**a*** and *MTL**α*** respectively (11). Thus, it is unclear if the up-regulation of non-mating genes is a *MTL* specific transcriptional nuance, or a feature of more highly virulent *C. auris* clades. The *MTL* also did not feature prominently in the filamentation response observed in clade V, providing no evidence for an obvious role for the *MTL* in such morphological changes.

Filamentation is an important pathogenicity trait in fungi, especially *Candida* species, although its roles have been more poorly described in aquatic infections (95). We observed *in vivo* filamentation by a representative strain of *C. auris* clade V, the basal/ancestral clade (96), accompanied by a genera-typical filamentous gene expression signature. Specifically, we measured the up-regulation of *HGC1* and *UME6*, which are two of the most important regulators of filamentation in *C. albicans*, and have recently been described as drivers of *C. auris* filamentation and biofilm formation (97). The expression of adhesin *SCF1* in filamenting clade V is noteworthy because its cationic adhesion mechanism has been postulated to be consistent with adhesion mechanisms common to marine organisms including bivalves (19). The generalist marine-isolated pathogen *C. haemulonii* has also displayed filamentation competence at lower temperatures (98), consistent with an ancestral aquatic state.

Human histopathology reports of *C. auris* infection are rarely published and have not demonstrated classical in-host filamentation, to our knowledge. An *ex vivo* human epithelial model using a clade I isolate did demonstrate filamentous *C. auris* at 37 °C after injection into deeper dermis (99). Clade III *C. auris* has also been observed to form filamentous/hyphal forms in *Galleria mellonella* injection (58). Fan and colleagues have observed filamentous forms of *C. auris* across all four clades, even demonstrating a higher virulence in the *G. mellonella* model (100), though the phenotype required passage through a murine host with additional prolonged growth at 25 °C for at least 5 d before and after injection (17). Other stimuli have induced filamentation in clade I isolates, such as hydroxyurea genotoxic stress (101) and Hsp90 inhibition (102), where several up-regulated genes in *C. auris* filamentation (*SCF1*, *IFF4* and *PGA31*) matched those in our study. Constitutive filamentous growth has also been demonstrated with a transposon-mediated disruption of a long non-coding RNA (103), which sit adjacent to chitin deacetylase *CDA2*, which was down-regulated at 24 HPI in our experiment during filamentation. These findings indicate that hyphal formation is possible across *C. auris* clades.

A total of twelve siderophore transporters were up-regulated during infection, and four were down-regulated, with three family members up-regulated in more virulent clades and five in the

filamentous clade V. The fact that siderophore transporter up-regulation has also been detected during *ex vivo* whole blood infection by *C. auris* underscores the likelihood that our findings are clinically relevant (28). Interestingly, this family of predicted xenosiderophore transporter genes is significantly expanded in several members of the *Metschnikowiaceae* clade compared to other *Saccharomycetae* (21), raising questions as to the roles of siderophore transporters in *C. auris* biology and evolution (104). Siderophore synthesis may be unlikely in *C. auris*, given the lack of evidence in other *Candida* species (105). As a result, *C. albicans* Sit1, which is required for virulence (106), is thought to be a xenosiderophore transporter for iron-chelators produced by other microbes and specific to the ferrioxamine type common in iron-poor ocean environments (107, 108). Siderophore transporters can also act intracellularly for compartments such as the mitochondrion (109, 110), or act as efflux pumps for various molecules (111) including trichothecene mycotoxins as identified by our functional annotations.

C. auris encodes a large expanded gene family of 17 siderophore transporters that we named xenosiderophore transporter candidates (*XTC*) 1-12 and haem transport-related (*HTR*) genes 1-5, the latter sharing sequence similarity with *S. pombe* low-affinity haem transporter Str3 (112). In other *Candida* species such as *C. albicans*, iron assimilation is understood to be central for in-host survival (113, 114), where deprivation triggers various pathogenic programmes such as alterations in cell surface beta-glucan (115). Haem is acquired by *C. albicans* through vesicular endocytosis and CFEM-domain containing proteins (116, 117) and does not contain *HTR* genes, suggesting a possible loss of transmembrane haem transporters. The ubiquity of *HTR* across the fungal kingdom and lack of *XTC* genes in the three basal fungal phyla suggest that *SIT1*/*HTC* could have arisen from a duplication of an *HTR*-related gene in the *Dikarya* (the *Ascomycota* and *Basidiomycota*) with subsequent independent loss of both *XTC* and *HTC* genes in multiple fungal lineages. Our identification of up-regulated *XTC* transport during infection corroborates the findings of up-regulated *XTC2A-B* (*B9J08_1547-8*) in an *ex vivo* blood model of *C. auris* infection (28). These findings together underline the importance of iron metabolism during infection, which could be targeted in the clinic, e.g. *via* low-toxicity pyrvinium pamoate (118, 119).

We show for the first time an *in vivo* infection host tissue transcriptional profile for the critical priority WHO human fungal pathogen *C. auris*. Representative strains from all five major clades of the recent simultaneous emergences highlighted strain-specific differences in morphology, virulence and gene expression. This study highlights the advantages and potential of a clinically relevant thermotolerant yolk-sac injection model, adding to the debate around the putative marine origins of *C. auris*, and the emergence of distinct clades. We demonstrate natural filamentation by clade V and virulence difference for clades I and IV, and comprehensively describe associated gene expression. We indicate the importance of the *XTC* and *HTR* gene clusters as recommended targets for investigation of fungal biology, pathogenicity and treatment. These gene mechanisms likely enable *C. auris* to survive in host

tissue and provide a step forward in understanding the pathobiology of an emerging fungal pathogen and global public health threat.

Materials and methods

Full details are given in SI Appendix. Briefly, wild-type adult AK were kept at the Aquatic Resources Facility, Exeter, under Project Licence PP4402521. AK were kept in two 28 °C incubation tanks, with 12-hour day and night light cycles and artificial enrichment foliage. Embryos were collected using three plastic netted collection chambers per tank. Injection needles were prepared using borosilicate glass capillaries (Harvard apparatus, USA) and a heated pulling system (heater level >62, PC-10, Narishige, UK). We used tweezers to snap the tip to an estimated 1 mm graticule-measured aperture of 10-20 µm, and sterilised needles before use with 253.7 nm UV light over 15 min (Environmental Validation Solutions, UK). Injection bays were made with microwaved 1% agarose (Sigma, UK) in 1 g per 100 mL ASW for up to 24 embryos in 100 mm petri dishes using custom-made molds in an inverted 60 mm petri dish. Embryos were randomly chosen from each dish and the sequence of injection for each biological repeat was randomly allocated by computer. *C. auris* yeasts were counted by haemocytometer and added to 25 µL sterile filtered phenol red solution 0.5% (Sigma, UK) to a concentration of 0.5×10^8 per mL in 100 µL. Injection needles were loaded with 5 µL injection solution using 20 µL Microloader EpT.I.P.S. (Eppendorf, UK) immediately before injection of up to 30 embryos before re-loading. Injections were performed with 400-500 hPa injection pressure and 7-40 hPa compensation pressure over 100-200 ms with the FemtoJet 4i (Eppendorf UK) using a micromanipulator (World Precision Instruments, UK) and a Microtec HM-3 stereo dissection microscope (Optech, UK). To deliver a dose of approx. 500 yeasts in 10 nL solution, an injection bolus was administered to an estimated diameter of 0.2 – 0.3 mm (10-15% of total embryo diameter) *via* a single chorion puncture. Any embryos that failed to meet these criteria for injection were excluded. Control *in vitro* inoculations were microinjected as above into 1 mL YPD in 1.5 mL Eppendorf tubes before incubation without shaking at 37 °C for 24 h contemporaneously with embryos as below.

We used an unblinded prospective virulence study comparing six groups of AK embryo yolk-sac microinjection, including clades I-V of *C. auris*, and sham injections as the negative control. We used ≥23 embryos per condition based on a power calculation of σ = 0.25, significance = 0.05, power = 0.9, and δ effect size of 25% mortality (two-sided t-test). After excluding embryos that were unhealthy or did not complete successful microinjection, We included n = 10-13 embryos per group per experiment (total n = 34-37 embryos per group). RNA was extracted from three embryos per condition per time-point (0, 24 and 48 HPI, n = 54) plus three embryos per time-point without any injection (n = 9, total n = 63) as a

control for the impact of microinjection.

We selected five *C. auris* strains to represent each major clade (**Table S1**). Culture stocks were kept in -80 °C in Yeast extract Peptone Dextrose (YPD) broth (Sigma-Aldrich, UK) containing 25% glycerol (ThermoFisher, UK) and plated onto YPD-agar (Sigma-Aldrich) for 48 h before inoculation and overnight growth in 10 mL YPD broth at 30 °C in a shaking incubator at 200 RPM (Multitron, Infors HT, UK). Five mL from each overnight culture was then centrifuged at 5000 g for 2 min before triple washing in 1 mL autoclaved deionised water (DIW, Milli-Q, Merck, USA) to prevent aggregation (20), then re-suspended again in 200 µL DIW.

Individual embryos were kept in 1 mL sterile filtered ASW per embryo in a 48 well flat bottom plate (Corning, USA) sealed with Parafilm “M” (Bemis Company, USA) at 37 °C with passive humidification using a 500 mL open glass beaker of water. Embryos were monitored for presence of heart rate at 24-hourly intervals up to 7 d by stereo dissection microscope. Initial time of injection was subtracted from each time-point to minimise bias between groups. Kaplan-Meier survival curves were plotted with Log-Rank testing and Benjamini-Hochberg (BH) correction (120) using survival v.3.5.8 and survminer v.0.4.9 packages in R v.4.4.0. Colony forming units (CFUs) were calculated by homogenisation of embryos at 0, 24, and 48 HPI by autoclaved plastic micropestle in a 1.5 mL conical tube (Eppendorf, UK) in 100 µL 10,000 U/mL penicillin/streptomycin (P/S) solution (Gibco, UK).

Dilutions were made with P/S solution and DIW in 1/10-10,000 and counts were adjusted according to dilution after plating onto YPD agar plates and read after 72 h incubation at 30 °C. Statistical testing between CFU numbers was performed with Wilcoxon testing and BH correction.

Total RNA was extracted using the Monarch® Total RNA Miniprep Kit (NEB, USA). Embryos were flash frozen in liquid nitrogen, re-suspended in DNA/RNA Protection Reagent and disrupted with an autoclaved plastic micropestle. Bead beating was performed in a FastPrep 24 homogeniser (MP Biomedicals) with 0.5 mm zirconia/silica beads for 8 cycles of 35 s at 6 m/s plus 45 s on ice. Lysate was recovered and incubated for 5 at 55 °C with proteinase K before addition of lysis buffer and RNA purification following manufacturer’s instructions. Library preparation and sequencing were performed by the Exeter Sequencing Service. Samples were normalised and prepared using the NEBNext Ultra II Directional RNA Library Prep - Poly(A) mRNA Magnetic Isolation Module following the standard protocol. Libraries were sequenced on a Novaseq 6000 sequencer with 150bp paired-end reads. Reads were trimmed with fastp (121) v.0.23.1 to remove reads <75 bases and trim based from the 3’ end with q-score <22. Quality control was performed with FastQC (https://github.com/s-andrews/FastQC) v.0.11.9 and

MultiQC (122) v.1.6.

We aligned sequences (x = 52.9 m reads per replicate, range 41.1-112.2 m) using the Trinity pipeline (123) v.2.15.1 to the *C. auris* clade I B8441 reference genome (GCA_002759435.2) (21) downloaded from GenBank (mean aligned reads in infected embryos 3.83 m, 0.81-13.1%). We further aligned clade-specific reference genomes for each strain (**Table S1**), including clade II (GCA_003013715.2) (4), III (GCA_002775015.1)(12), IV (GCA_008275145.1)(12) and V (GCA_016809505.1)(96, 124, 125). We aligned conditions containing *A. dispar* to the *de novo* GJEY01 adult gill transcriptome assembly (84) downloaded from GenBank, for which we detected expression over 27,481 potential genes. Alignment was performed with Bowtie2 (126) v.2.5.1, transcript estimation with RNA Seq by Expectation Maximisation (RSEM) (127) v.1.3.3, differential expression with EdgeR (128) v.3.40.0, Samtools (129) v.1.17 and limma (130) v.3.54.0 using a false discovery rate (FDR) p-value cut-off of 0.001 and a log fold change cut-off of +/-2.0. Principal components were calculated and plotted using the prcomp function in Rv4.4.0 and ggfortify v.0.4.17 R package for fragments per kilobase per million, and correlations plots from counts per million as per the default output of the Trinity pipeline. Log fold change was plotted with ComplexHeatmap (131).

Gene ontology terms (132, 133) were assigned using DIAMOND (134) v.2.1.8 *via* the DIAMOND2GO pipeline (135) for each of the *C. auris* reference genomes. KEGG terms (136) were assigned using the BlastKOALA online platform using the eukaryote database (137). Protein FAMily (PFAM) domains (138) were identified using the PFAM-A.hmm database (https://ftp.ebi.ac.uk/pub/databases/Pfam/current_release/Pfam-A.full.gz) and HMMER and HMM Scan (139) with a cut-off of $1e^{-5}$. Further domain-specific identification was performed with SignalP 5.0 (140), DeepTMHMM 1.0 (141) and NetGPI 1.1 (142). To identify accessory genes across *C. auris* clades, we used the Synima pipeline (143) with Orthofinder v2.5.5 (144) with additional reference genomes for *C. albicans* (SC5314_GCA_000182965.3) and *C. haemulonii* (B11899_ASM1933202v1). Multiple alignment of single copy orthologues as defined by Orthofinder was performed with Muscle v5.1 (145) and a phylogeny was made with FastTree v2.1.11 (146). We visualised the structure using Alphafold v3 (147) and ChimeraX v1.8 (148). Clade I-V *C. auris* and *C. haemulonii SIT1* genes were aligned using Muscle as above before using RAXML-NG v1.2.2 with 1000 bootstraps and the LG4X model (149), which was visualised using ggtree v3.12.0.

Data availability: Raw reads have been deposited *via* NCBI/GEO *via* accession GSE277854. All datasets and code required to make figures are available *via* Github (https://github.com/hughgifford/Arabian_Killifish_C_auris_2024).

Acknowledgements

We acknowledge funding from the MRC Centre for Medical Mycology at the University of Exeter (MR/N006364/2, MR/V033417/1), MRC Doctoral Training Grants MR/P501955/2 and MR/W502649/1, Wellcome Trust (206412/A/17/Z), Wellcome Trust Career Development Award (215239/Z/19/Z) and Wellcome Trust Fellowship (219551/Z/19/Z), National Centre for the Replacement, Refinement and Reduction of Animals in Research (NC3Rs) (NC/X001121/1), and the NIHR Exeter Biomedical Research Centre. TB also was supported *via* Elizabeth Ballou and a Sir Henry Dale Fellowship jointly funded by the Wellcome Trust and the Royal Society (211241/Z/18/Z) and the Lister Institute. The views expressed are those of the authors and not necessarily those of the NIHR or the Department of Health and Social Care. We thank staff in the Aquatic Resource Center at the University of Exeter for husbandry of the fish and the support for developing protocols for feeding, spawning, and raising new generations of this relatively new model species, including Sam Worthington, Chloe Flint and Richard Silcox. We also thank the Exeter Sequencing Service facility and support from Wellcome Trust Institutional Strategic Support Fund (WT097835MF), Wellcome Trust Multi User Equipment Awards (WT101650MA and 218247/Z/19/Z), Medical Research Council Clinical Infrastructure Funding (MR/M008924/1) and BBSRC LOLA award (BB/K003240/1). We also thank the University of Exeter High-Performance Computing (HPC) facility funded by the UK MRC Clinical Research Infrastructure Initiative (award number MR/M008924/1). We thank Tanmoy Chakraborty, Dhara Malavia and Neil Gow for providing *C. auris* strains, Teigan Veale, Sumita Roy, Jonathan Ball and Darren Thomson for assistance in microscopy and Chloe Pelletier for advice on aggregation. We also thank Microtechnical Services, Exeter, UK, for assistance with histological sectioning.

References

1. J. F. Meis, A. Chowdhary, *Candida auris*: A global fungal public health threat. *The Lancet Infectious Diseases* **18**, 1298–1299 (2018).

2. WHO, World Health Organisation (WHO) fungal priority pathogens list to guide research, development and public health action. (2022). https://doi.org/https://www.who.int/publications/i/item/9789240060241.

3. W. G. Lee, *et al.*, First three reported cases of nosocomial fungemia caused by *Candida auris*. *Journal of Clinical Microbiology* **49**, 4 (2011).

4. K. Satoh, *et al.*, *Candida auris* sp. Nov., a novel ascomycetous yeast isolated from the external ear canal of an inpatient in a Japanese hospital. *Microbiology and Immunology* **53**, 41–44 (2009).

5. D. W. Eyre, *et al.*, A *Candida auris* outbreak and its control in an intensive care setting. *New England Journal of Medicine* **379**, 1322–1331 (2018).

6. S. K. Taori, *et al.*, *Candida auris* outbreak: Mortality, interventions and cost of sustaining control. *Journal of Infection* **79**, 601–611 (2019).

7. L. Shuping, *et al.*, High prevalence of *Candida auris* colonization during protracted neonatal unit outbreak, South Africa. *Emerging Infectious Diseases* (2023). https://doi.org/10.3201/eid2909.230393.

8. R. D. Adam, *et al.*, Analysis of *Candida auris* fungemia at a single facility in Kenya. *International Journal of Infectious Diseases* **85**, 182–187 (2019).

9. P. S. Prayag, S. Patwardhan, S. Panchakshari, P. A. Rajhans, A. Prayag, The dominance of *Candida auris*: A single-center experience of 79 episodes of candidemia from western India. *Indian Journal of Critical Care Medicine* **26**, 560–563 (2022).

10. T. Khan, *et al.*, Emergence of the novel sixth *Candida auris* clade VI in Bangladesh. *Microbiology Spectrum* **12**, e03540–23 (2024).

11. C. Suphavilai, *et al.*, Detection and characterisation of a sixth *Candida auris* clade in Singapore: A genomic and phenotypic study. *Lancet Microbe* **0** (2024).

12. S. R. Lockhart, *et al.*, Simultaneous emergence of multidrug-resistant *Candida auris* on 3 continents confirmed by whole-genome sequencing and epidemiological analyses. *Clinical Infectious Diseases* **64**, 134–140 (2017).

13. H. Gifford, J. Rhodes, R. A. Farrer, The diverse genomes of *Candida auris*. *The Lancet Microbe* **0** (2024).

14. S. A. Byun, *et al.*, Virulence traits and azole resistance in Korean *Candida auris* Isolates. *Journal of Fungi* **9**, 979 (2023).

15. D. J. Santana, G. Zhao, T. R. O'Meara, The many faces of *Candida auris*: Phenotypic and strain variation in an emerging pathogen. *PLOS Pathogens* **20**, e1012011 (2024).

16. J. Chen, *et al.*, Is the superbug fungus really so scary? A systematic review and meta-analysis of global epidemiology and mortality of *Candida auris*. *BMC Infectious Diseases* **20**, 827 (2020).

17. H. Yue, *et al.*, Filamentation in *Candida auris*, an emerging fungal pathogen of humans: Passage through the mammalian body induces a heritable phenotypic switch. *Emerging Microbes & Infections* **7**, 1–13 (2018).

18. C. Chadwick, M. D. Jesus, F. Ginty, J. S. Martinez, Pathobiology of *Candida auris* infection analyzed by multiplexed imaging and single cell analysis. *PLOS ONE* **19**, e0293011 (2024).

19. D. J. Santana, *et al.*, A *Candida auris*-specific adhesin, Scf1, governs surface association, colonization, and virulence. *Science* **381**, 1461–1467 (2023).

20. C. Pelletier, S. Shaw, S. Alsayegh, A. J. P. Brown, A. Lorenz, *Candida auris* undergoes adhesin-dependent and -independent cellular aggregation. *PLOS Pathogens* **20**, e1012076 (2024).

21. J. F. Muñoz, *et al.*, Genomic insights into multidrug-resistance, mating and virulence in *Candida auris* and related emerging species. *Nature Communications* **9**, 5346 (2018).

22. J. P. Richardson, *et al.*, Candidalysins are a new family of cytolytic fungal peptide toxins. *mBio* **13**, e03510–21 (2022).

23. J.-S. Kim, K.-T. Lee, Y.-S. Bahn, Secreted aspartyl protease 3 regulated by the Ras/cAMP/PKA pathway promotes the virulence of *Candida auris*. *Frontiers in Cellular and Infection Microbiology* **13**, 1257897 (2023).

24. M. V. Horton, *et al.*, *Candida auris* cell wall mannosylation contributes to neutrophil evasion through pathways divergent from *Candida albicans* and *Candida glabrata*. *mSphere* **6**, e00406–21 (2021).

25. H. Weerasinghe, *et al.*, *Candida auris* uses metabolic strategies to escape and kill macrophages while avoiding robust activation of the NLRP3 inflammasome response. *Cell Reports* **42**, 112522 (2023).

26. M. Lyman, Notes from the field: Transmission of pan-resistant and echinocandin-resistant *Candida auris* in health care facilities - Texas and the District of Columbia, January-April 2021. *Morbidity and Mortality Weekly Report* **70** (2021).

27. T. W. Wang, *et al.*, Functional redundancy in *Candida auris* cell surface adhesins crucial for cell-cell interaction and aggregation. *Nature Communications* **15**, 9212 (2024).

28. S. Allert, *et al.*, From environmental adaptation to host survival: Attributes that mediate pathogenicity of *Candida auris*. *Virulence* **13**, 191–214 (2022).

29. B. Fayed, *et al.*, Transcriptome analysis of human dermal cells infected with *Candida auris* identified unique pathogenesis/defensive mechanisms particularly ferroptosis. *Mycopathologia* **189**, 65 (2024).

30. B. Yang, *et al.*, A correlative study of the genomic underpinning of virulence traits and drug tolerance of *Candida auris*. *Infection and Immunity* **0**, e00103–24 (2024).

31. A. Balakumar, *et al.*, Single-cell transcriptomics unveils skin cell specific antifungal immune responses and IL-1Ra- IL-1R immune evasion strategies of emerging fungal pathogen *Candida auris*. *PLOS Pathogens* **20**, e1012699 (2024).

32. M. Bruno, *et al.*, Transcriptional and functional insights into the host immune response against the emerging fungal pathogen *Candida auris*. *Nature Microbiology* **5**, 1516–1531 (2020).

33. Y. Wang, *et al.*, Innate immune responses against the fungal pathogen *Candida auris*. *Nature Communications* **13**, 3553 (2022).

34. X. Wang, *et al.*, The first isolate of *Candida auris* in China: Clinical and biological aspects. *Emerging Microbes & Infections* **7**, 1–9 (2018).

35. S. Fan, C. Li, J. Bing, G. Huang, H. Du, Discovery of the diploid form of the emerging fungal pathogen *Candida auris*. *ACS Infectious Diseases* **6**, 2641–2646 (2020).

36. S. Fan, *et al.*, A biological and genomic comparison of a drug-resistant and a drug-susceptible strain of *Candida auris* isolated from Beijing, China. *Virulence* **12**, 1388–1399 (2021).

37. S. Wurster, N. D. Albert, D. P. Kontoyiannis, *Candida auris* bloodstream infection induces upregulation of the PD-1/PD-L1 immune checkpoint pathway in an immunocompetent mouse model. *mSphere* **7**, e00817–21 (2022).

38. J. Bing, *et al.*, Rapid evolution of an adaptive multicellular morphology of *Candida auris* during systemic infection. *Nature Communications* **15**, 2381 (2024).

39. R. Ben-Ami, *et al.*, Multidrug-resistant *Candida haemulonii* and *C. auris*, Tel Aviv, Israel. *Emerging Infectious Diseases* **23** (2017).

40. C. L. Hager, E. L. Larkin, L. A. Long, M. A. Ghannoum, Evaluation of the efficacy of rezafungin, a novel echinocandin, in the treatment of disseminated *Candida auris* infection using an immunocompromised mouse model. *Journal of Antimicrobial Chemotherapy* **73**, 2085–2088 (2018).

41. M. Zhao, *et al.*, *In vivo* pharmacokinetics and pharmacodynamics of APX001 against *Candida* spp. In a neutropenic disseminated candidiasis mouse model. *Antimicrobial Agents and Chemotherapy* **62**, e02542–17 (2018).

42. S. Singh, *et al.*, The NDV-3A vaccine protects mice from multidrug resistant *Candida auris* infection. *PLOS Pathogens* **15**, e1007460 (2019).

43. F. Zhang, *et al.*, A marine microbiome antifungal targets urgent-threat drug-resistant fungi. *Science* **370**, 974–978 (2020).

44. J. E. Muñoz, *et al.*, Pathogenicity levels of Colombian strains of *Candida auris* and Brazilian strains of *Candida haemulonii* species complex in both murine and *Galleria mellonella* experimental models. *Journal of Fungi* **6**, 104 (2020).

45. M. Abe, *et al.*, Potency of gastrointestinal colonization and virulence of *Candida auris* in a murine endogenous candidiasis. *PLoS One* **15**, e0243223 (2020).

46. L. Forgács, *et al.*, Comparison of in vivo pathogenicity of four *Candida auris* clades in a neutropenic bloodstream infection murine model. *Emerging Microbes & Infections* **9**, 1160–1169 (2020).

47. F. Nagy, *et al.*, In vitro and in vivo interaction of caspofungin with isavuconazole against *Candida auris* planktonic cells and biofilms. *Medical Mycology* **59**, 1015–1023 (2021).

48. L. Forgács, *et al.*, In vivo efficacy of amphotericin B against four *Candida auris* clades. *Journal of Fungi (Basel, Switzerland)* **8**, 499 (2022).

49. S. Singh, *et al.*, Protective efficacy of anti-Hyr1p monoclonal antibody against systemic candidiasis due to multi-drug-resistant *Candida auris*. *Journal of Fungi* **9**, 103 (2023).

50. E. A. Salama, *et al.*, Lansoprazole interferes with fungal respiration and acts synergistically with amphotericin B against multidrug-resistant *Candida auris*. *Emerging Microbes & Infections* **13**, 2322649 (2024).

51. S. R. Torres, *et al.*, Impact of *Candida auris* infection in a neutropenic murine model. *Antimicrobial Agents and Chemotherapy* **64**, e01625–19 (2020).

52. H. Xin, F. Mohiuddin, J. Tran, A. Adams, K. Eberle, Experimental mouse models of disseminated *Candida auris* infection. *mSphere* **4**, e00339–19 (2019).

53. J. Rosario-Colon, K. Eberle, A. Adams, E. Courville, H. Xin, *Candida* cell-surface-specific monoclonal antibodies protect mice against *Candida auris* invasive infection. *International Journal of Molecular Sciences* **22**, 6162 (2021).

54. S. R. Torres, *et al.*, Assessment of environmental and occupational exposure while working with multidrug resistant (MDR) fungus *Candida auris* in an animal facility. *Journal of Occupational and Environmental Hygiene* **16**, 507–518 (2019).

55. A. M. Borman, Of mice and men and larvae: *Galleria mellonella* to model the early host-pathogen interactions after fungal infection. *Virulence* **9**, 9–12 (2017).

56. D. Romera, *et al.*, The *Galleria mellonella* infection model as a system to investigate the virulence of *Candida auris* strains. *Pathogens and Disease* **78**, ftaa067 (2020).

57. L. C. García-Carnero, *et al.*, Early virulence predictors during the *Candida* species–*Galleria mellonella* interaction. *Journal of Fungi* **6**, 152 (2020).

58. V. Garcia-Bustos, *et al.*, Characterization of the differential pathogenicity of *Candida auris* in a *Galleria mellonella* infection model. *Microbiology Spectrum* **9**, e00013–21 (2021).

59. S. K. Carvajal, *et al.*, Pathogenicity assessment of Colombian strains of *Candida auris* in the *Galleria mellonella* invertebrate model. *Journal of Fungi* **7**, 401 (2021).

60. A. Hernando-Ortiz, *et al.*, Virulence of *Candida auris* from different clinical origins in *Caenorhabditis elegans* and *Galleria mellonella* host models. *Virulence* **12**, 1063–1075 (2021).

61. K. Spettel, *et al.*, *Candida auris* in Austria—what is new and what is different. *Journal of Fungi* **9**, 129 (2023).

62. S. Wurster, *et al.*, *Drosophila melanogaster* as a model to study virulence and azole treatment of the emerging pathogen *Candida auris*. *Journal of Antimicrobial Chemotherapy* **74**, 1904–1910 (2019).

63. V. Harpf, G. Rambach, R. Würzner, C. Lass-Flörl, C. Speth, *Candida* and complement: New aspects in an old battle. *Frontiers in Immunology* **11**, 1471 (2020).

64. J. Pechacek, M. S. Lionakis, Host defense mechanisms against *Candida auris*. *Expert Review of Anti-infective Therapy* **21**, 1087–1096 (2023).

65. L. Bavia, L. E. Santiesteban-Lores, M. C. Carneiro, M. M. Prodocimo, Advances in the complement system of a teleost fish, *Oreochromis niloticus*. *Fish & Shellfish Immunology* **123**, 61–74 (2022).

66. K. Buchmann, A. M. Karami, Y. Duan, The early ontogenetic development of immune cells and organs in teleosts. *Fish & Shellfish Immunology* **146**, 109371 (2024).

67. H. Tian, *et al.*, Cytokine networks provide sufficient evidence for the differentiation of CD4+ T cells in teleost fish. *Developmental & Comparative Immunology* **141**, 104627 (2023).

68. C. J. Johnson, J. M. Davis, A. Huttenlocher, J. F. Kernien, J. E. Nett, Emerging fungal pathogen *Candida auris* evades neutrophil attack. *mBio* **9**, e01403–18 (2018).

69. S. Pharkjaksu, N. Boonmee, C. Mitrpant, P. Ngamskulrungroj, Immunopathogenesis of emerging *Candida auris* and *Candida haemulonii* strains. *Journal of Fungi* **7**, 725 (2021).

70. R. S. Shapiro, L. E. Cowen, Uncovering cellular circuitry controlling temperature-dependent fungal morphogenesis. *Virulence* **3**, 400–404 (2012).

71. M. D. Leach, *et al.*, Hsf1 and Hsp90 orchestrate temperature-dependent global transcriptional remodelling and chromatin architecture in *Candida albicans*. *Nature Communications* **7**, 11704 (2016).

72. W. Xiao, *et al.*, Response and regulatory mechanisms of heat resistance in pathogenic fungi. *Applied Microbiology and Biotechnology* **106**, 5415–5431 (2022).

73. A. Akbarzadeh, E. H. Leder, Acclimation of killifish to thermal extremes of hot spring: Transcription of gonadal and liver heat shock genes. *Comparative Biochemistry and Physiology Part A: Molecular & Integrative Physiology* **191**, 89–97 (2016).

74. A. Hamied, *et al.*, Identification and characterization of highly fluorescent pigment cells in embryos of the Arabian killifish (*Aphanius Dispar*). *iScience* **23**, 101674 (2020).

75. A. Alsakran, *et al.*, Stage-by-stage exploration of normal embryonic development in the Arabian killifish, *Aphanius dispar*. *Developmental Dynamics* **n/a** (2024).

76. R. Minhas, *et al.*, The thermotolerant Arabian killifish, *Aphanius dispar*, as a novel infection model for human fungal pathogens. 2024.10.08.617174 (2024).

77. P. Arora, *et al.*, Environmental isolation of *Candida auris* from the coastal wetlands of Andaman Islands, India. *mBio* **12**, e03181–20 (2021).

78. P. Escandón, Novel environmental niches for *Candida auris*: Isolation from a coastal habitat in Colombia. *Journal of Fungi* **8**, 748 (2022).

79. V. Uden, M. C. Kolipinski, *Torulopsis haemulonii nov. spec.*, A yeast from the Atlantic Ocean. *Antonie Van Leeuwenhoek* **28**, 78–80 (1962).

80. N. Burden, K. Chapman, F. Sewell, V. Robinson, Pioneering better science through the 3Rs: An introduction to the national centre for the replacement, refinement, and reduction of animals in research (NC3Rs). *Journal of the American Association for Laboratory Animal Science* **54**, 198–208 (2015).

81. M. S. Skrzypek, *et al.*, The *Candida* Genome Database (CGD): Incorporation of Assembly 22, systematic identifiers and visualization of high throughput sequencing data. *Nucleic Acids Research* **45**, D592–D596 (2017).

82. J. Potrykus, *et al.*, Fungal iron availability during deep seated candidiasis is defined by a complex interplay involving systemic and local events. *PLOS pathogens* **9**, e1003676 (2013).

83. L. Kasper, *et al.*, The fungal peptide toxin candidalysin activates the NLRP3 inflammasome and causes cytolysis in mononuclear phagocytes. *Nature Communications* **9**, 4260 (2018).

84. L. C. Bonzi, *et al.*, The time course of molecular acclimation to seawater in a euryhaline fish. *Scientific Reports* **11**, 18127 (2021).

85. A. Varma, *et al.*, Molecular cloning and functional characterisation of a glucose transporter, CaHGT1, of *Candida albicans*. *FEMS microbiology letters* **182**, 15–21 (2000).

86. L. Luo, X. Tong, P. C. Farley, The *Candida albicans* gene *HGT12* (Orf19.7094) encodes a hexose transporter. *FEMS Immunology & Medical Microbiology* **51**, 14–17 (2007).

87. V. Brown, J. A. Sexton, M. Johnston, A glucose sensor in Candida albicans. *Eukaryotic Cell* **5**, 1726–1737 (2006).

88. D. E. Larcombe, *et al.*, Glucose-enhanced oxidative stress resistance-A protective anticipatory response that enhances the fitness of *Candida albicans* during systemic infection. *PLOS Pathogens* **19**, e1011505 (2023).

89. R. Martin, *et al.*, A core filamentation response network in *Candida albicans* is restricted to eight genes. *PLOS ONE* **8**, e58613 (2013).

90. S. S. Schatzman, *et al.*, Copper-only superoxide dismutase enzymes and iron starvation stress in *Candida* fungal pathogens. *The Journal of Biological Chemistry* **295**, 570–583 (2020).

91. J. M. Rybak, *et al.*, Abrogation of triazole resistance upon deletion of *CDR1* in a clinical isolate of *Candida auris*. *Antimicrobial Agents and Chemotherapy* **63** (2019).

92. J. Li, A. T. Coste, D. Bachmann, D. Sanglard, F. Lamoth, Deciphering the Mrr1/Mdr1 pathway in azole resistance of *Candida auris*. *Antimicrobial Agents and Chemotherapy* **66**, e00067–22 (2022).

93. S. Sun, M. A. Coelho, M. David-Palma, S. J. Priest, J. Heitman, The evolution of sexual reproduction and the mating-type locus: Links to pathogenesis of *Cryptococcus* human pathogenic fungi. *Annual Review of Genetics* **53**, 417–444 (2019).

94. Y. Wang, J. Xu, Population genomic analyses reveal evidence for limited recombination in the superbug *Candida auris* in nature. *Computational and Structural Biotechnology Journal* **20**, 3030–3040 (2022).

95. D. P. Overy, T. Rämä, R. Oosterhuis, A. K. Walker, K.-L. Pang, The neglected marine fungi, *Sensu stricto*, and their isolation for natural products' discovery. *Marine Drugs* **17**, 42 (2019).

96. N. A. Chow, *et al.*, Potential fifth clade of *Candida auris,* Iran, 2018. *Emerging Infectious Diseases* **25**, 1780–1781 (2019).

97. M. Louvet, *et al.*, Ume6-dependent pathways of morphogenesis and biofilm formation in *Candida auris*. *Microbiology Spectrum* **0**, e01531–24 (2024).

98. Y. Deng, S. Li, J. Bing, W. Liao, L. Tao, Phenotypic switching and filamentation in *Candida haemulonii*, an emerging opportunistic pathogen of humans. *Microbiology Spectrum* **9**, e00779–21 (2021).

99. S. Seiser, *et al.*, Native human and mouse skin infection models to study *Candida auris*-host interactions. *Microbes and Infection* **26**, 105234 (2024).

100. S. Fan, *et al.*, Filamentous growth is a general feature of *Candida auris* clinical isolates. *Medical Mycology* **59**, 734–740 (2021).

101. G. Bravo Ruiz, Z. K. Ross, N. A. R. Gow, A. Lorenz, Pseudohyphal growth of the emerging pathogen *Candida auris* is triggered by genotoxic stress through the S phase checkpoint. *mSphere* **5**, e00151–20 (2020).

102. S. H. Kim, *et al.*, Genetic analysis of *Candida auris* implicates Hsp90 in morphogenesis and azole tolerance and Cdr1 in Azole Resistance. *mBio* **10**, e02529–18 (2019).

103. J. Gao, *et al.*, LncRNA DINOR is a virulence factor and global regulator of stress responses in *Candida auris*. *Nature Microbiology* **6**, 842–851 (2021).

104. A. D. Chybowska, D. S. Childers, R. A. Farrer, Nine things genomics can tell us about *Candida auris*. *Frontiers in Genetics* **11**, 351 (2020).

105. A. Ismail, G. W. Bedell, D. M. Lupan, Siderophore production by the pathogenic yeast, *Candida albicans*. *Biochemical and Biophysical Research Communications* **130**, 885–891 (1985).

106. P. Heymann, *et al.*, The Siderophore iron transporter of *Candida albicans* (Sit1p/Arn1p) mediates uptake of ferrichrome-type siderophores and Is required for epithelial invasion. *Infection and Immunity* **70**, 5246–5255 (2002).

107. R. M. Boiteau, *et al.*, Siderophore-based microbial adaptations to iron scarcity across the eastern Pacific Ocean. *Proceedings of the National Academy of Sciences* **113**, 14237–14242 (2016).

108. J. Park, *et al.*, Siderophore production and utilization by marine bacteria in the North Pacific Ocean. *Limnology and Oceanography* **68**, 1636–1653 (2023).

109. J. C. Renshaw, *et al.*, Fungal siderophores: Structures, functions and applications. *Mycological Research* **106**, 1123–1142 (2002).

110. T. C. Johnstone, E. M. Nolan, Beyond iron: Non-classical biological functions of bacterial siderophores. *Dalton Transactions* **44**, 6320–6339 (2015).

111. Y. Nakajima, *et al.*, Effect of disrupting the trichothecene efflux pump encoded by *FgTri12* in the nivalenol chemotype of *Fusarium graminearum*. *The Journal of General and Applied Microbiology* **61**, 93–96 (2015).

112. P. Xue, *et al.*, Heme sensing and trafficking in fungi. *Fungal Biology Reviews* **43**, 100286 (2023).

113. R. Fourie, O. O. Kuloyo, B. M. Mochochoko, J. Albertyn, C. H. Pohl, Iron at the Centre of *Candida albicans* Interactions. *Frontiers in Cellular and Infection Microbiology* **8**, 185 (2018).

114. A. Alselami, R. A. Drummond, How metals fuel fungal virulence, yet promote anti-fungal immunity. *Disease Models & Mechanisms* **16**, dmm050393 (2023).

115. A. Pradhan, *et al.*, Non-canonical signalling mediates changes in fungal cell wall PAMPs that drive immune evasion. *Nature Communications* **10**, 5315 (2019).

116. Z. Weissman, D. Kornitzer, A family of *Candida* cell surface haem-binding proteins involved in haemin and haemoglobin-iron utilization. *Molecular Microbiology* **53**, 1209–1220 (2004).

117. C. Ding, *et al.*, Conserved and divergent roles of Bcr1 and CFEM proteins in *Candida parapsilosis and Candida albicans*. *PLOS ONE* **6**, e28151 (2011).

118. C. Simm, *et al.*, Disruption of iron homeostasis and mitochondrial metabolism are promising targets to inhibit *Candida auris*. *Microbiology Spectrum* **10**, e00100–22 (2022).

119. J. Zhang, *et al.*, Pyrvinium pamoate synergizes with azoles *in vitro* and *in vivo* to exert antifungal efficacy against *Candida auris* and other *Candida* species. *Infection and Drug Resistance* **18**, 783–789 (2025).

120. Y. Benjamini, Y. Hochberg, Controlling the false discovery rate: A practical and powerful approach to multiple testing. *Journal of the Royal Statistical Society Series B: Statistical Methodology* **57**, 289–300 (1995).

121. S. Chen, Y. Zhou, Y. Chen, J. Gu, Fastp: An ultra-fast all-in-one FASTQ preprocessor. *Bioinformatics* **34**, i884–i890 (2018).

122. P. Ewels, M. Magnusson, S. Lundin, M. Käller, MultiQC: Summarize analysis results for multiple tools and samples in a single report. *Bioinformatics* **32**, 3047–3048 (2016).

123. B. J. Haas, *et al.*, De novo transcript sequence reconstruction from RNA-seq using the Trinity platform for reference generation and analysis. *Nature Protocols* **8**, 1494–1512 (2013).

124. M. Abastabar, *et al.*, *Candida auris* otomycosis in Iran and review of recent literature. *Mycoses* **62**, 101–105 (2019).

125. J. F. Muñoz, *et al.*, Clade-specific chromosomal rearrangements and loss of subtelomeric adhesins in *Candida auris*. *Genetics* **218**, iyab029 (2021).

126. B. Langmead, S. L. Salzberg, Fast gapped-read alignment with Bowtie 2. *Nature Methods* **9**, 357–359 (2012).

127. B. Li, C. N. Dewey, RSEM: Accurate transcript quantification from RNA-Seq data with or without a reference genome. *BMC Bioinformatics* **12**, 323 (2011).

128. M. D. Robinson, D. J. McCarthy, G. K. Smyth, edgeR: A Bioconductor package for differential expression analysis of digital gene expression data. *Bioinformatics* **26**, 139–140 (2010).

129. H. Li, *et al.*, The Sequence Alignment/Map format and SAMtools. *Bioinformatics* **25**, 2078–2079 (2009).

130. M. E. Ritchie, *et al.*, Limma powers differential expression analyses for RNA-sequencing and microarray studies. *Nucleic Acids Research* **43**, e47 (2015).

131. Z. Gu, R. Eils, M. Schlesner, Complex heatmaps reveal patterns and correlations in multidimensional genomic data. *Bioinformatics* **32**, 2847–2849 (2016).

132. M. Ashburner, *et al.*, Gene Ontology: Tool for the unification of biology. *Nature Genetics* **25**, 25–29 (2000).

133. The Gene Ontology Consortium, *et al.*, The Gene Ontology knowledgebase in 2023. *Genetics* **224**, iyad031 (2023).

134. B. Buchfink, K. Reuter, H.-G. Drost, Sensitive protein alignments at tree-of-life scale using DIAMOND. *Nature Methods* **18**, 366–368 (2021).

135. C. Golden, D. J. Studholme, R. A. Farrer, DIAMOND2GO: A rapid Gene Ontology assignment and enrichment tool for functional genomics. 2024.08.19.608700 (2024).

136. M. Kanehisa, M. Furumichi, Y. Sato, M. Kawashima, M. Ishiguro-Watanabe, KEGG for taxonomy-based analysis of pathways and genomes. *Nucleic Acids Research* **51**, D587–D592 (2022).

137. M. Kanehisa, Y. Sato, K. Morishima, BlastKOALA and GhostKOALA: KEGG tools for functional characterization of genome and metagenome sequences. *Journal of Molecular Biology* **428**, 726–731 (2016).

138. A. Bateman, *et al.*, The Pfam protein families database. *Nucleic Acids Research* **32**, D138–D141 (2004).

139. S. R. Eddy, Accelerated profile HMM searches. *PLOS Computational Biology* **7**, e1002195 (2011).

140. J. J. Almagro Armenteros, *et al.*, SignalP 5.0 improves signal peptide predictions using deep neural networks. *Nature Biotechnology* **37**, 420–423 (2019).

141. J. Hallgren, *et al.*, DeepTMHMM predicts alpha and beta transmembrane proteins using deep neural networks. (2022).

142. M. H. Gíslason, H. Nielsen, J. J. Almagro Armenteros, A. R. Johansen, Prediction of GPI-anchored proteins with pointer neural networks. *Current Research in Biotechnology* **3**, 6–13 (2021).

143. R. A. Farrer, Synima: A synteny imaging tool for annotated genome assemblies. *BMC Bioinformatics* **18**, 507 (2017).

144. D. M. Emms, S. Kelly, OrthoFinder: Phylogenetic orthology inference for comparative genomics. *Genome Biology* **20**, 238 (2019).

145. R. C. Edgar, MUSCLE: Multiple sequence alignment with high accuracy and high throughput. *Nucleic Acids Research* **32**, 1792–1797 (2004).

146. M. N. Price, P. S. Dehal, A. P. Arkin, FastTree 2 – approximately maximum-likelihood trees for large alignments. *PLOS ONE* **5**, e9490 (2010).

147. J. Abramson, *et al.*, Accurate structure prediction of biomolecular interactions with AlphaFold 3. *Nature* **630**, 493–500 (2024).

148. E. F. Pettersen, *et al.*, UCSF ChimeraX: Structure visualization for researchers, educators, and developers. *Protein Science* **30**, 70–82 (2021).

149. A. Stamatakis, RAxML version 8: A tool for phylogenetic analysis and post-analysis of large phylogenies. *Bioinformatics* **30**, 1312–1313 (2014).

Figures and Tables

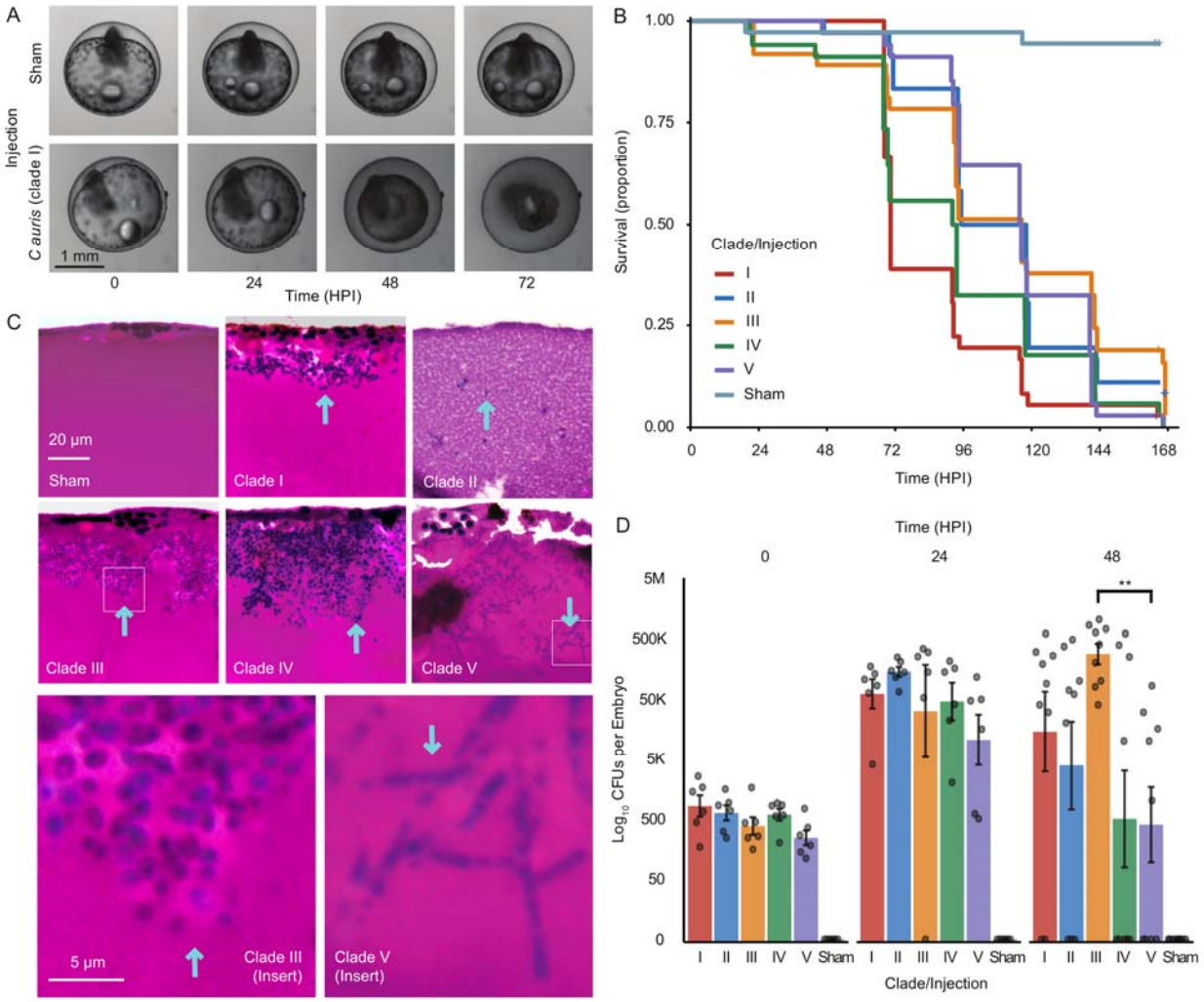

Figure 1: Modelling *C. auris* infection in the Arabian killifish **(A)** Illustrative time-lapse microscopy of embryo death including yolk-sac collapse during infection (clade I infection) or survival (sham injection) using Acquifer live imaging. **(B)** Survival curves for embryos injected with each *C. auris* clade or sham injection. Significance testing between groups is given in **Table S1**; hours post injection (HPI). **(C)** H&E Staining of AK yolk-sac at 48 HPI for each clade or sham injection; morphology is indicated by blue arrows, with insets indicating typical yeast (clade III) and filamentous morphology (clade V). The yolk-sac edge is oriented at the top. **(D)** Colony forming units (CFUs) per clade from embryos homogenised after injection as an indicator of injection dose and *in vivo* growth.

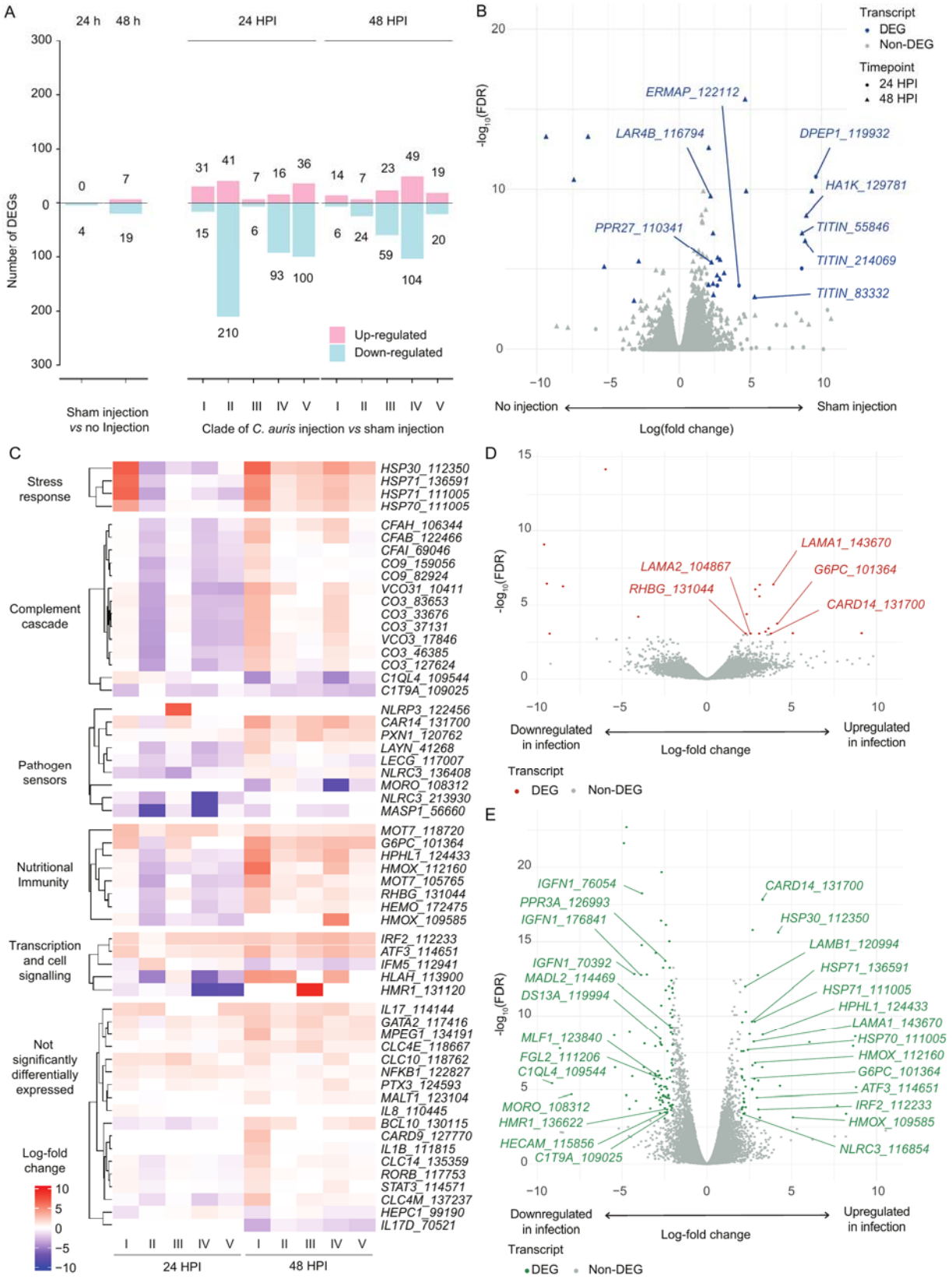
A
24 h
48 h
24 HPI
48 HPI
Number of DEGs
Up-regulated
Down-regulated
Sham injection vs no Injection
Clade of C. auris injection vs sham injection
B
Transcript
DEG
Non-DEG
Timepoint
24 HPI
48 HPI
-log10(FDR)
ERMAP_122112
LAR4B_116794
DPEP1_119932
HA1K_129781
PPR27_110341
TITIN_55846
TITIN_214069
TITIN_83332
No injection
Sham injection
Log(fold change)
C
Stress response
Complement cascade
Pathogen sensors
Nutritional Immunity
Transcription and cell signalling
Not significantly differentially expressed
Log-fold change
HSP30_112350
HSP71_136591
HSP71_111005
HSP70_111005
CFAH_106344
CFAB_122466
CFAI_69046
CO9_159056
CO9_82924
VCO31_10411
CO3_83653
CO3_33676
CO3_37131
VCO3_17846
CO3_46385
CO3_127624
C1QL4_109544
C1T9A_109025
NLRP3_122456
CAR14_131700
PXN1_120762
LAYN_41268
LECG_117007
NLRC3_136408
MORO_108312
NLRC3_213930
MASP1_56660
MOT7_118720
G6PC_101364
HPHL1_124433
HMOX_112160
MOT7_105765
RHBG_131044
HEMO_172475
HMOX_109585
IRF2_112233
ATF3_114651
IFM5_112941
HLAH_113900
HMR1_131120
IL17_114144
GATA2_117416
MPEG1_134191
CLC4E_118667
CLC10_118762
NFKB1_122827
PTX3_124593
MALT1_123104
IL8_110445
BCL10_130115
CARD9_127770
IL1B_111815
CLC14_135359
RORB_117753
STAT3_114571
CLC4M_137237
HEPC1_99190
IL17D_70521
24 HPI
48 HPI
D
-log10(FDR)
LAMA1_143670
LAMA2_104867
G6PC_101364
RHBG_131044
CARD14_131700
Downregulated in infection
Upregulated in infection
Log-fold change
Transcript
DEG
Non-DEG
E
-log10(FDR)
IGFN1_76054
CARD14_131700
PPR3A_126993
HSP30_112350
IGFN1_176841
LAMB1_120994
IGFN1_70392
HSP71_136591
MADL2_114469
HSP71_111005
DS13A_119994
HPHL1_124433
LAMA1_143670
MLF1_123840
HSP70_111005
FGL2_111206
HMOX_112160
C1QL4_109544
G6PC_101364
ATF3_114651
MORO_108312
IRF2_112233
HMR1_136622
HMOX_109585
HECAM_115856
NLRC3_116854
C1T9A_109025
Downregulated in infection
Upregulated in infection
Log-fold change
Transcript
DEG
Non-DEG

Figure 2: AK host responses to *C. auris* infection: **(A)** Number of differentially expressed genes (DEGs) for each of two comparisons, sham injection *vs* no injection (left panel), and *C. auris* injection *vs* sham injection (right panel), at either 24 or 48 h post injection (HPI). **(B)** Volcano plot showing log-fold change and significance according to $-\log^{10}$ false discovery rate (FDR) for sham injection *vs* no injection. **(C)** Heatmap demonstrating log-fold change for differential expression between *C. auris* injection and sham injection for groups of genes. **(D)** Volcano plot showing log-fold change and significance for DEGs expressed during infection with clade I *C. auris* at 48 HPI. **(E)** Volcano plot showing log-fold change and significance for DEGs expressed during infection with clade IV *C. auris* at 48 HPI.

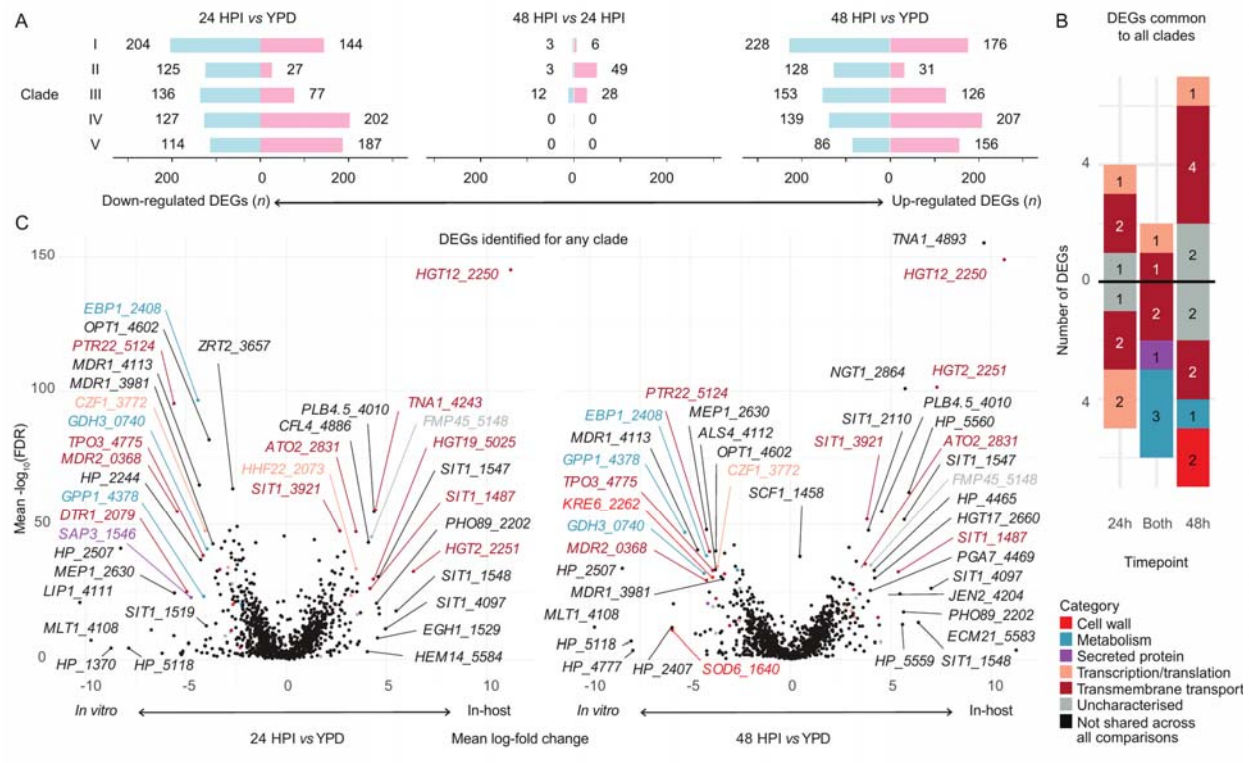

Figure 3: *C. auris* gene expression *in vivo vs in vitro* **(A)** Total DEGs per clade for each comparison between 24 h post injection (HPI), 48 HPI, and growth in YPD alone. **(B)** Combined set of significant DEGs common to all five clades between *in vivo* infection and *in vivo* growth in YPD. Genes are coloured by manually annotated category (**Table S3**). **(C)** Volcano plots demonstrate mean log-fold change for DEGs identified for any clade. Genes with infinite false discovery rate (FDR) are indicated with an arrow. Genes included in the combined set are coloured by category as per panel **B**.

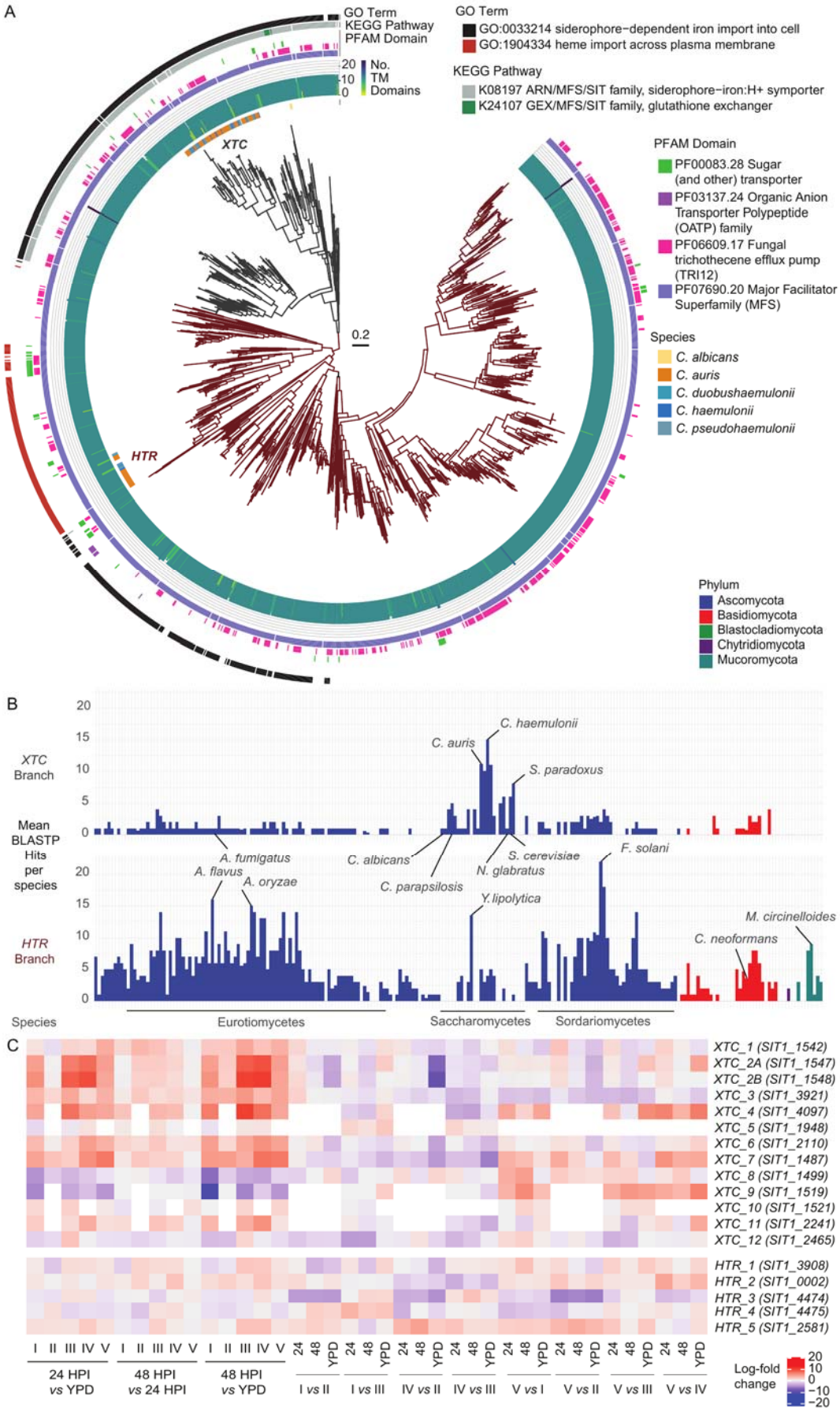
A
GO Term
KEGG Pathway
PFAM Domain
20
10
0
No. TM Domains
GO Term
GO:0033214 siderophore−dependent iron import into cell
GO:1904334 heme import across plasma membrane
KEGG Pathway
K08197 ARN/MFS/SIT family, siderophore−iron:H+ symporter
K24107 GEX/MFS/SIT family, glutathione exchanger
XTC
HTR
0.2
PFAM Domain
PF00083.28 Sugar (and other) transporter
PF03137.24 Organic Anion Transporter Polypeptide (OATP) family
PF06609.17 Fungal trichothecene efflux pump (TRI12)
PF07690.20 Major Facilitator Superfamily (MFS)
Species
C. albicans
C. auris
C. duobushaemulonii
C. haemulonii
C. pseudohaemulonii
Phylum
Ascomycota
Basidiomycota
Blastocladiomycota
Chytridiomycota
Mucoromycota
B
XTC Branch
Mean BLASTP Hits per species
HTR Branch
C. haemulonii
C. auris
S. paradoxus
A. fumigatus
A. flavus
A. oryzae
C. albicans
C. parapsilosis
S. cerevisiae
N. glabratus
Y. lipolytica
F. solani
M. circinelloides
C. neoformans
Species
Eurotiomycetes
Saccharomycetes
Sordariomycetes
C
XTC_1 (SIT1_1542)
XTC_2A (SIT1_1547)
XTC_2B (SIT1_1548)
XTC_3 (SIT1_3921)
XTC_4 (SIT1_4097)
XTC_5 (SIT1_1948)
XTC_6 (SIT1_2110)
XTC_7 (SIT1_1487)
XTC_8 (SIT1_1499)
XTC_9 (SIT1_1519)
XTC_10 (SIT1_1521)
XTC_11 (SIT1_2241)
XTC_12 (SIT1_2465)
HTR_1 (SIT1_3908)
HTR_2 (SIT1_0002)
HTR_3 (SIT1_4474)
HTR_4 (SIT1_4475)
HTR_5 (SIT1_2581)
24 HPI vs YPD
48 HPI vs 24 HPI
48 HPI vs YPD
I vs II
I vs III
IV vs II
IV vs III
V vs I
V vs II
V vs III
V vs IV
Log-fold change

Figure 4: Panfungal Xenosiderophore Phylogeny of **(A)** Blastp hits for *C. albicans SIT1* across fungal genomes available in FungiDB. Sssequeunces were aligned with Clustal Omega and FastTreee, scale bar: substitutions per site, *XTC*: xenosiderophore transport candidate, *HTR*: haem transport-related. **(B)** Per-species mean Blastp hits for siderophore transporters. **(C)** Differential expression of *XTC/HTR* genes assigned in order of B8441 v3 contig across experiments in this paper.